



Hydrogenolysis of glycerol to propanediols over silicotungstic acid catalysts intercalated with CuZnFe hydrotalcite-like compounds

Ruiping Wei^a, Xumin Qu^a, Yang Xiao^{b,*}, Jingdeng Fan^a, Gaoli Geng^a, Lijing Gao^a, Guomin Xiao^{a,*}

^a School of Chemistry and Chemical Engineering, Southeast University, Nanjing 211189, Jiangsu, China

^b Davidson School of Chemical Engineering, Purdue University, West Lafayette, IN 47907, United States

ARTICLE INFO

Keywords:

Hydrogenolysis of glycerol
1,3-Propanediols (1,3-PDO)
1,2-Propanediols (1,2-PDO)
Hydrotalcite-like compounds (HTLCs)
Silicotungstic acid (SiW)

ABSTRACT

A series of catalysts derived from silicotungstic acid (SiW) intercalated with CuZnFe hydrotalcite-like compounds (HTLCs) via ion-exchange method was prepared and characterized by N₂-physisorption, XRD, TEM, SEM, H₂-TPR, FT-IR, and Py-IR spectra. The intercalation of SiW species into CuZnFe HTLCs was confirmed by these characterization techniques, while the catalytic performance was evaluated for glycerol hydrogenolysis. It was found that introduction of SiW significantly enhanced the selectivity towards 1,3-propanediols (1,3-PDO), owing to the increased Brønsted acid introduction, as demonstrated by Py-IR analysis. The catalyst intercalating 30 wt. % SiW showed the highest selectivity (22.4%) to 1,3-PDO at 68.9% glycerol transformation. The catalytic performance was discussed and correlated with the physicochemical properties of these catalysts. The present contribution provides an economical approach to convert surplus glycerol from biodiesel manufacture to valuable propanediols.

1. Introduction

A by-product of the biodiesel manufacture industry – glycerol is generated in great amounts due to the growing application of biodiesel as a renewable fuel. The large surplus glycerol is an important bio-refinery chemical since glycerol purification cost has rapidly dropped [1–5]. The application approach development to make good utilization of surplus glycerol would greatly benefit the biodiesel manufacturing industry. Many efforts have been devoted to converting glycerol into valuable chemicals, such as acrolein, propanediols, glycol, glyceric acid, acrylic acid, *in situ* hydrogen, hydrocarbon fuels, and additional specialty chemicals [6–11]. Among these products, converting glycerol to 1, 2-propanediol (1,2-PDO) and/or 1,3-propanediol (1,3-PDO), catalytically selective hydrogenolysis has attracted much attention in the recent decade [12–14]. As the main monomer of polypropylene terephthalate, 1,3-PDO provides higher value than its isomer – 1,2-PDO [15]. Two producing routes of 1,3-PDO synthesis have been reported as follows: a hydration process starting from acrolein (Degussa-DuPont), and a hydroformylation process of ethylene oxide (Shell) [16]. Owing to the unstable price of petroleum and limited resource availability, however, these routes are costly and maybe not followed in the future. Therefore,

converting byproduct glycerol of biodiesel manufacture into propanediols, in particular, 1,3-PDO is of great development prospect.

1,2-PDO and 1,3-PDO formation as glycerol hydrogenolysis products is typically via two different pathways, as illustrated in Scheme 1. Over acidic catalysts, glycerol dehydration at the primary and secondary –OH occur over Brønsted and Lewis acid sites, respectively, leading to hydroxyacetone and 3-hydroxypropanal, which are further converted to 1,2- and 1,3-PDO via hydrogenation [17–19], respectively. Interestingly, when initial dehydration of glycerol occurs at secondary-OH over Brønsted acid sites, 1,3-PDO formation is still challenging since it competes with further dehydration over the same Brønsted acid sites that produces acrolein. It indicates that a moderate number of Brønsted acid sites must be carefully designed to achieve relatively high yield and selectivity to 1,3-PDO.

Heteropoly acids (HPAs) and/or acid salts possess strong Brønsted acidity, which has been reported conducive to the dehydration of secondary alcohol [20]. Raw HPAs, however, as homogeneous catalysts are limited by their low surface area and thermal stability. Many efforts thus have been devoted to supported HPAs, leading to heterogeneous catalysts. Nakagawa et al. [21] reported 1,3-PDO formation from the conversion of glycerol over an Ir–Re bimetallic catalyst, achieving 38% 1,

* Corresponding authors.

E-mail addresses: xiao63@purdue.edu (Y. Xiao), xiaogm@seu.edu.cn (G. Xiao).

<https://doi.org/10.1016/j.cattod.2020.11.028>

Received 2 December 2019; Received in revised form 15 September 2020; Accepted 4 November 2020

Available online 30 January 2021

0920-5861/© 2021 Elsevier B.V. All rights reserved.

3-PDO yield when the H₂ pressure was 8 MPa. Feng et al. [22] made Al- and W-incorporated SiO₂ and SBA-15 materials, where they showed favorable catalytic performance (50% selectivity towards 1,3-PDO at a 66% conversion of glycerol) in selective hydrogenolysis of glycerol, due to the three-component synergistic effect in the support. Kurosaka et al. [23] reported glycerol hydrogenolysis to 1,3-PDO over a Pt-W/ZrO₂ catalyst, achieving 24% selectivity toward 1,3-PDO, while glycerol conversion was only 14.2%. In addition, the use of 1,3-dimethyl-2-imidazolidinone as an organic solvent has limited its broad applications. Using relatively low (5 wt.%) glycerol aqueous solution, Garcia-Fernandez et al. [24] reported glycerol conversion to 1,3-PDO over a Pt/WO_x/Al₂O₃ catalyst, reaching 51.9% selectivity to 1,3-PDO at the conversion 53.1% of glycerol at 220 °C and 4.5 MPa H₂ initial pressure. HTLCs, or hydrotalcite-like compounds, i.e., LDHs (layered double hydroxides), have been broadly used in various areas [25–30]. HTLCs consist of alternative cationic [M_(1-x)^{II}M_x^{III}(OH)₂]^{x+} and anionic A^{x-}·zH₂O layers. The layers were positively charged, which contain the edge-shared hydroxide octahedra M^{II} and M^{III}, in which the charges are neutralized by A^{x-} in interlayer space. HPAs containing a Keggin structure are ideal candidates as molecule-building blocks for various material preparation [31].

In spite of relatively high 1,3-PDO yields, the application of high boiling-point organic solvent and relatively high operating pressure greatly reduce the environmental viability of 1,3-PDO production. In our prior work, we have focused on non-noble metal catalysts for glycerol conversion to propanediols such as Cu/ZnO-USY, Cu-MgO/USY, and Cu-Ca-Al hydrotalcite derived catalysts [25–27]. It was found that 1,3-PDO selectivity was enhanced by both Brønsted and Lewis acid sites, which was also closely related to acid-base composite supports. In the present work, catalysts derived from silicotungstic acid (SiW) intercalated with CuZnFe HTLC via ion-exchange were prepared, characterized and evaluated for glycerol hydrogenolysis. We demonstrated that with the optimal intercalating amount of SiW into CuZnFe HTLC, the selectivity toward 1,3-PDO was greatly improved, likely owing to the moderate number of Brønsted acid sites.

2. Experimental

2.1. Chemicals

The following compounds were purchased from Sinopharm Chemical Reagent Co. Ltd., China: sodium hydroxide (NaOH), copper(II) nitrate trihydrate (Cu(NO₃)₂·3H₂O), zinc(II) nitrate hexahydrate (Zn(NO₃)₂·6H₂O), iron(III) nitrate nonahydrate (Fe(NO₃)₃·9H₂O), silicotungstic acid hydrate (H₄W₁₂SiO₄₀·xH₂O), glycerol, and ethanol. The products including 1,3- and 1,2-propanediol (1,3- and 1,2-PDO), and internal standard 1,4-butanediol were obtained from Shanghai Lingfeng Chemical Reagent Co. Ltd., China.

2.2. Catalyst preparation

Using the co-precipitation method, CuZnFe hydrotalcite-like compound was prepared. Briefly, metal nitrates as precursors with the desired Cu:Zn:Fe molar ratio 3:12:5 were dissolved in 100 mL H₂O. A NaOH-containing solution (3.2 mol/L) was prepared before co-precipitation. With vigorous mechanical stirring and an inert N₂ flowing, both of the above solutions were dropwise added into 20 mL H₂O at 65 °C, maintaining pH ~10. The precipitate was aged over-night with vigorous stirring at 65 °C, followed by vacuum filtration and rinsing by water until pH approached 7. This material is denoted as CuZnFeH-NO₃, while it was denoted as CuZnFe after calcination for 4 h at 500 °C. To perform intercalation, desired amounts (10–40 wt.%) of silicotungstic acid (SiW) and 5 g CuZnFeH-NO₃ were both charged into a sealed vessel with pH 4–4.5 at 110 °C for 4 h. Then it was filtered, rinsed, dried, and then calcined for 4 h at 500 °C, leading to CuZnFe-xSiW, where x (wt.%) indicated the mass fraction of SiW.

2.3. Catalyst characterization

Using Rigaku D/max-A instrument, the powder X-ray diffraction, i.e., XRD, patterns were recorded with a Cu Kα radiation at 8 °/min scan speed 30 mA and 50 kV, 30 mA. FT-IR (Fourier-transform infrared

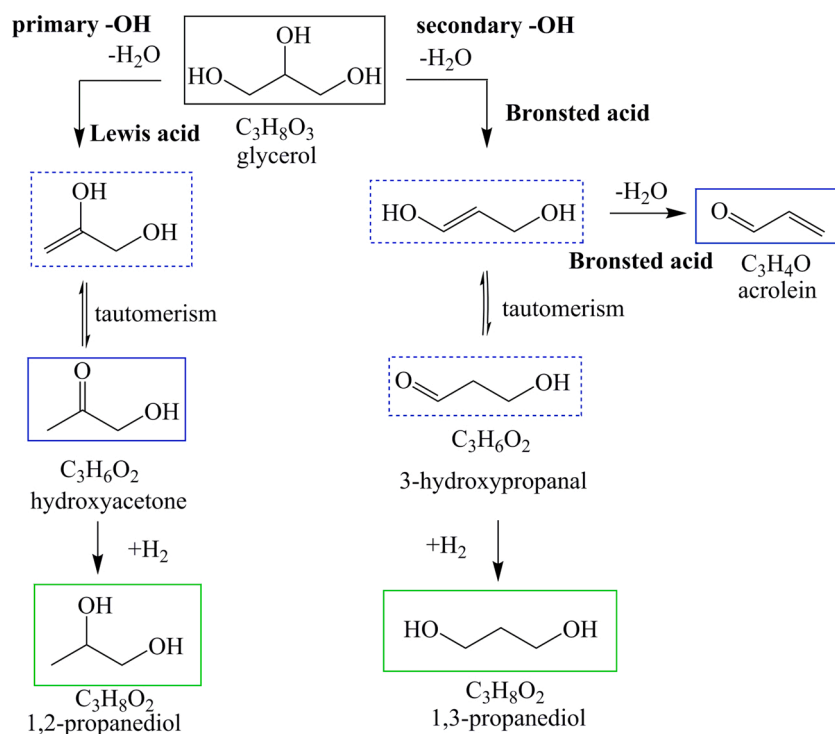


Fig. 1. Glycerol hydrogenolysis network, blue: dehydration products; green: hydrogenolysis products; solid frame: experimentally found products; dash frame: proposed intermediates.

spectroscopy) 1 was conducted on TENSOR27 with KBr spectrophotometer at 400–2000 cm^{-1} . Prior to SEM (scanning electron microscopy) scans, samples were spray-gold pre-treated, followed by on Hitachi S-4800 instrument using 15 kV as the accelerating voltage. EDX (energy dispersive X-ray) spectrum was utilized to obtain metallic element distribution. TEM, i.e., transmission electron microscopy, was scanned on a Tecnai G2-20 instrument after a sample was well dispersed in ethanol solution followed by being placed onto 400 mesh C-covered Cu grid, and drying for 15 min. Py-IR (pyridine adsorption Fourier-transform infrared spectroscopy) were employed on NEXUS after the sample was well pressed into a wafer, followed by moving into the infrared quartz cell. The samples were additionally pre-treated for 2 h at 300 °C under a vacuum condition. Upon cooled to 120 °C, pyridine was quantitatively flowing into the cell, while the spectra were recorded after pyridine had desorbed for 15 min at 300 °C. The redox property was measured by H_2 -hydrogen temperature-programmed reduction, noted as H_2 -TPR, using a TP-5076 instrument. Typically, after 0.05 g sample was pre-treated in He flow for 1 h at 400 °C, and cooled to 100 °C, a TPR profile was recorded at 100–500 °C with 10 °C/min ramping rate and 10% H_2/N_2 flow. The surface area was measured using the standard N_2 adsorption-desorption isotherms, in a Beishide 3H-2000 analyzer instrument via N_2 physisorption at 77 K after degassing for 12 h at 393 K under vacuum condition. The surface area was then calculated based on multipoint Brunauer-Emmett-Teller method.

2.4. Catalytic performance evaluation

Glycerol hydrogenolysis was conducted in an autoclave (200 mL total volume and stainless material) with an electromagnetic stirrer. The catalyst was activated in a H_2 flowing environment for 2 h at 300 °C. For a standard glycerol hydrogenolysis transformation, 100 g 40 wt.% glycerol in water solution with a known amount catalyst were placed into the autoclave. To replace air, the reactor was purged by N_2 for three times and H_2 for an additional three times. To eliminate the external diffusion effect 600 rpm stirring rate was applied. All catalysts powders were sieved to 80–100 mesh, eliminating the internal diffusion effect. The high pressure was carefully released after the reactor temperature was cooled to room temperature when the reaction was complete. The liquid was separated from the solid catalyst by centrifugation, followed by analysis using a gas chromatography (GC-6890) equipped with a capillary column (50 m \times 0.32 mm \times 0.5 μm , remarked as SE-54) and a flame ionization detector. The oven temperature was constantly set at 170 °C, while temperatures were 300 and 280 °C at injector and detector, respectively. 1,4-Butanediol was used as the internal standard for quantitative analysis.

3. Results and discussion

3.1. Results of catalyst characterization

Fig. 2 show XRD patterns of CuZnFeH-NO_3 and CuZnFeH-xSiW ($x = 10$ –40%) precursors before calcination, in which characteristic reflections of layered double hydroxides (LDHs) were detected in CuZnFeH-NO_3 sample, as assigned to $2\theta = 10.2^\circ$ (003), and $2\theta = 20.4^\circ$ (006), respectively [32]. Upon intercalating SiW via the ion exchange method, the diffractive peaks of layered double hydroxides in CuZnFeH-SiW samples shifted to lower angles at $2\theta = 7.7^\circ$ (003), and $2\theta = 11.9^\circ$ (006). This is because the size of heteropoly anion is greater than nitrate ion, thus the insertion of heteropoly anion leads to larger interlayer space [33,34]. Note that Fig. 2 confirms the successful intercalation of SiW into CuZnFe . The XRD patterns of CuZnFe , CuZnFe-30SiW catalysts after calcination at 500 °C and the raw SiW compound are shown in Fig. 3. It appears that characteristic reflections of layered double hydroxides disappeared after calcination, owing to dehydration and decomposition of anions during the calcination process, leading to the formation of multiple phases [35] as follows. Reflections at 31.9° , 34.5° ,

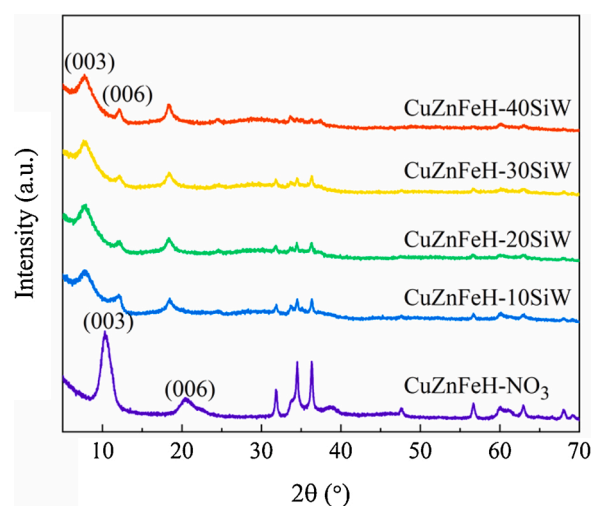


Fig. 2. XRD patterns for CuZnFeH-NO_3 and CuZnFeH-xSiW precursor.

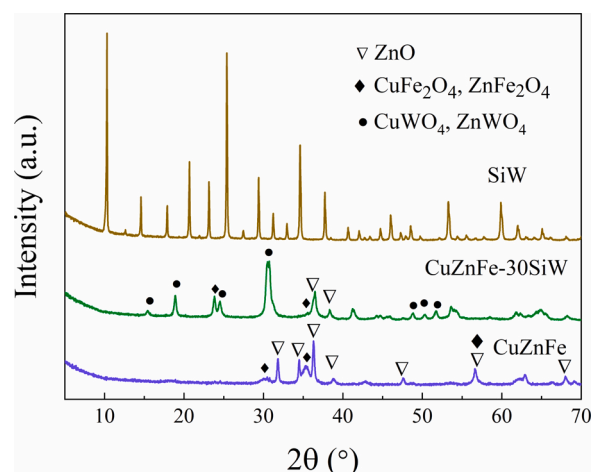


Fig. 3. XRD patterns for CuZnFe , CuZnFe-30SiW and SiW samples.

36.2° , and 38.7° correspond to the ZnO structure, while reflections at 30.3° , 35.2° , and 42.6° correspond to multiple phases CuFe_2O_4 and/or ZnFe_2O_4 . In addition, characteristic peaks of CuWO_4 and/or ZnWO_4 were also detected in the CuZnFe-30SiW sample. The surface area and pore volume values were listed in Table 1. The surface area increased from 37.9 to 42.1 m^2/g after SiW exchange with NO_3^- and continued to increase exchanging more SiW. This should be attributed to the larger size of Keggin structure of SiW than NO_3^- , which could increase the distance between the layers of CuZnFe HTLCs. However, the pore volume and size pore trends showed a different pattern due to the accumulation of SiW and disassemble CuZnFe .

The FT-IR spectra of CuZnFeH-NO_3 and CuZnFeH-SiW precursors, as well as the raw SiW sample are displayed in Fig. 4. The strong absorption band at 1618 cm^{-1} is assigned to the O–H asymmetrical stretching vibration of interlayer water. The absorption bands at 1382 and 838 cm^{-1}

Table 1
Physicochemical properties of various CuZnFe samples.

Catalyst	Surface area (m^2/g)	Pore volume (cm^3/g)	Pore size (nm)
CuZnFe	37.9	0.37	38.7
CuZnFe-10SiW	42.1	0.56	52.9
CuZnFe-20SiW	44.3	0.32	26.0
CuZnFe-30SiW	49.5	0.28	25.6
CuZnFe-40SiW	54.0	0.21	15.8

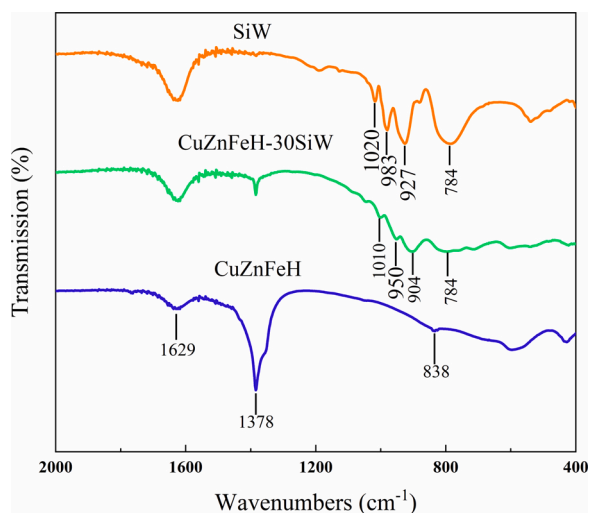


Fig. 4. FT-IR spectra for CuZnFeH-NO₃, CuZnFeH-30SiW and SiW samples.

are N–O asymmetrical stretching vibration of the nitrate ion. When NO₃⁻ was partially replaced by SiW, the characteristic absorption band of N–O at 1382 cm⁻¹ was obviously weakened, while the band at 838 cm⁻¹ disappeared. The characteristic vibrations of Keggin bands appeared in the range 700–1100 cm⁻¹. Absorption bands at 1010 and 784 cm⁻¹ correspond to the stretching vibrations of Si=O and Si–O–Si. Absorption bands at 950 and 904 cm⁻¹ are the asymmetrical stretching vibration of W=O and W–O–W, respectively. As compared with the raw SiW material, a part of characteristic vibrations of Keggin bands showed redshifts, which was likely caused by the interaction between SiW and CuZnFe slabs [36].

Fig. 5(a)–(d) shows SEM scans for CuZnFeH-NO₃ precursor, CuZnFe, CuZnFeH-30SiW precursor, and CuZnFe-30SiW. The layer structure of CuZnFeH-NO₃, as shown in Fig. 5(a), was with a sharp edge and defined orientation. Fig. 5(b) exhibits a relatively uniform hexagonal platelet-like sheet for the CuZnFeH-30SiW sample. The crystalline size of CuZnFeH-30SiW is greater than that of the original CuZnFeH due to recrystallization of the amorphous parts and small crystalline during the hydrothermal treatment of the ion exchange process [37]. After calcination, the lamellar structure of CuZnFe (see Fig. 5(c)) is partially destroyed, and the interlamination is filled with formed small particles. In addition, denser packing of the formed multiple phases was observed from Fig. 5(d), showing larger particles as compared with CuZnFe. To evaluate the composition of different CuZnFe and CuZnFe-xSiW catalysts, the element mapping was carried out and showed in Fig. 5(e)–(l), which described that Cu, Zn, Fe elements in the CuZnFe materials and Cu, Zn, Fe, Si, W elements in CuZnFe-30SiW catalysts were all uniformly distributed. Fig. 6 shows the Py-IR spectra of CuZnFe and CuZnFe-30SiW catalysts. Both spectra showed bands at 1540 cm⁻¹ owing to pyridinium ions adsorbed on Brønsted sites, and 1455 cm⁻¹ due to pyridinium ions on Lewis sites. It appears that the introduction of SiW significantly increases both Brønsted acid and Lewis acid sites.

The reductive performance of these materials was investigated by H₂-TPR. Fig. 7 compares H₂-TPR profiles of various catalysts. The profile of CuZnFe exhibits a single and broad reduction peak, denoted as α with the maximum H₂ consumption temperature at 233 °C. This peak is attributed to the one-step reduction of Cu²⁺ to Cu⁰ [38]. When the amount of SiW is increased, the reduction temperature for CuZnFe-xSiW catalysts shifted to a higher position, owing to its stronger interaction with more copper species. Interestingly, the CuZnFe-40SiW sample displays two reduction peaks, denoted as α and β . The α -peak is the reduction of highly dispersed CuO as well as isolated copper(II) clusters, while the β -peak is the reduction of intermediate copper(I) species to metallic copper species [39,40]. Fig. 8 shows TEM scans of freshly

reduced CuZnFe and CuZnFe-30SiW catalysts. Fig. 8(a) demonstrates that well-dispersed copper, leading to relatively small particles, is observed in a typical TEM scan. The CuZnFe-30SiW catalyst in Fig. 8(b), however, resulted in lower Cu dispersion with relatively uniform particle size. The above observation is consistent with H₂-TPR analysis in Fig. 7.

3.2. Results of catalytic performance

The catalytic performance of CuZnFe and CuZnFe-xSiW materials are compared in Table 2. It appears that the introduction of SiW into CuZnFe remarkably improved the selectivity as well as the yield of 1,3-PDO. When CuZnFe was used for glycerol hydrogenolysis, the yield of 1,3-PDO was only 6.4%, which increased to 9.2–15.4% when 10–30 wt.% SiW was introduced, while it caused the decrease of 1,2-PDO yield from 47.5% to 24.5%. Hydrogenolysis of glycerol involves many reactions as showed in Scheme 1. In order to achieve high selectivity towards different desired products, such as 1,3-PDO and 1,2-PDO, many works have been done to promote the desired reactions while inhibiting undesired reactions. The propanediol selectivity depends on various factors including catalyst active species, operating conditions and promoters. Generally, as demonstrated by Py-IR, the incorporation of SiW can be ascribed to the generation of Brønsted acid sites, which benefits the dehydration of the secondary –OH group in glycerol to produce 1,3-PDO. [41] When the amount of SiW continued to increase to 40 wt.%, the yield of 1,3-PDO decreased dramatically to 9.5%. As discussed in our prior review article [9], this observation is consistent with the strategy that a moderate number of Brønsted acid site benefit 1, 3-PDO formation, since too many Brønsted acid sites lead to further dehydration product acrolein (see Scheme 1). As the CuZnFe-30SiW catalyst exhibited the highest 1,3-PDO yield, in later sections this material was used to investigate the effects of reaction time, initial hydrogen pressure, as well as reaction temperature on the conversion and selectivity of glycerol hydrogenolysis. The catalyst has been reused for three times, catalyst deactivation was not observed, indicating stability of the HT structure.

Fig. 9 shows the effect of reaction time on glycerol hydrogenolysis. Glycerol conversion dramatically increased from 24.6% to 68.9% as the reaction time varied from 4 to 11 h, then it increased slowly. The selectivity values towards 1,2-PDO and 1,3-PDO both increased initially, while they exhibited decreasing trends when the reaction time continued to increase. Note that 1,2-PDO and 1,3-PDO reached their highest yields at 6 and 11 h, respectively, which implies that 1,3-PDO production is more difficult than 1,2-PDO. As 1,3-PDO is our primary target product, further investigations on operating conditions were carried out at 11 h as the reaction time.

The effect of reaction operating temperature on glycerol hydrogenolysis was studied at 160–230 °C (see Fig. 10). The conversion of glycerol was improved obviously from 22.8% to 68.9% as reaction temperature varied from 160 to 220 °C. This is likely due to that the initial dehydration of glycerol is an endothermic process, thus higher temperature promoted glycerol conversion in terms of thermodynamics. The selectivity to 1,2-PDO reached maximum at 180 °C, while the highest selectivity to 1,3-PDO was obtained at 220 °C. The above observation is in accordance with the literature that the formation of 1,3-PDO requires higher activation energy [42]. Therefore, 220 °C was selected as the optimal operating reaction temperature.

The operating pressure was varied from 2 to 4 MPa to investigate the effect of initial hydrogen pressure on glycerol hydrogenolysis, (Fig. 11). It is found that glycerol conversion increased gradually with hydrogen pressure. The selectivity values to 1,2-PDO and 1,3-PDO both increased from 13.2% to 35.6% and 11.5% to 22.4%. This could be explained in term of kinetics that as gaseous hydrogen solubility in the solution was enhanced by higher hydrogen pressure, more hydrogen was available to be adsorbed on the catalyst surface, leading to the rise of selectivity towards 1,2-PDO and 1,3-PDO [43]. Both 1,2-PDO and 1,3-PDO

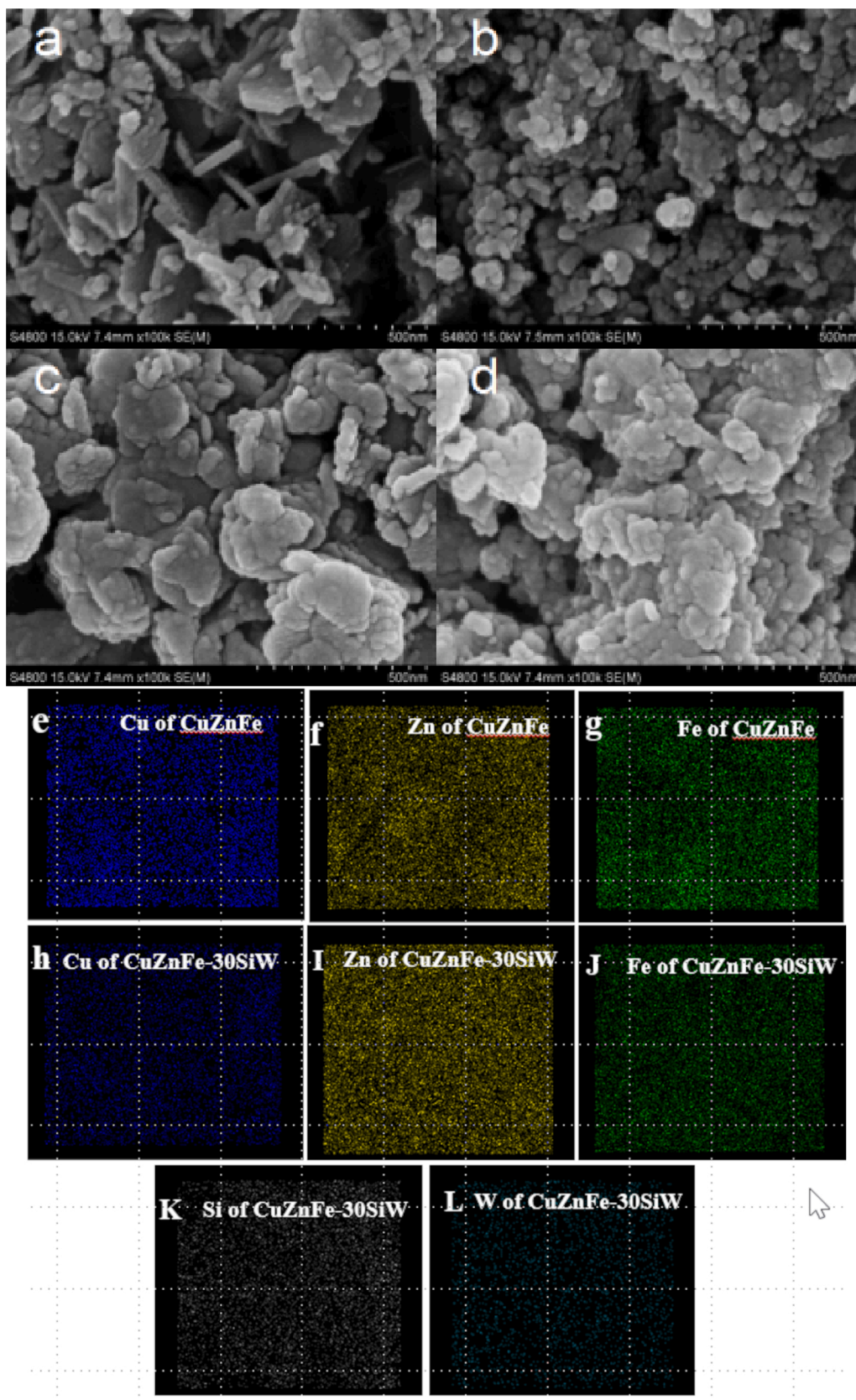


Fig. 5. SEM scans for (a) CuZnFeH-NO₃, (b) CuZnFe, (c) CuZnFeH-30SiW, (d) CuZnFe-30SiW, and (e)–(l) images of elemental mapping of CuZnFe and CuZnFe-30SiW.

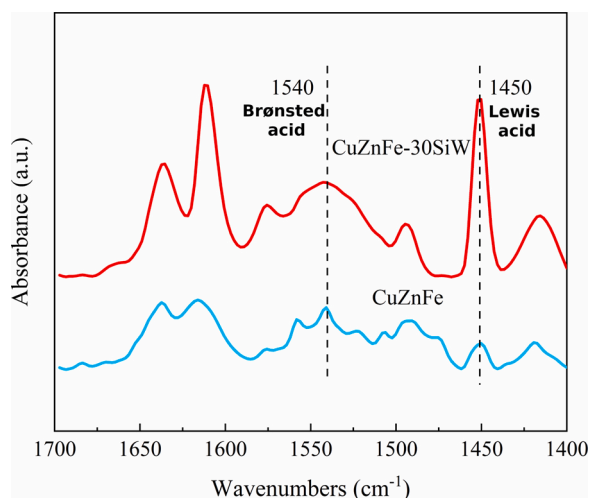


Fig. 6. Py-IR spectra for CuZnFe and CuZnFe-30SiW catalysts.

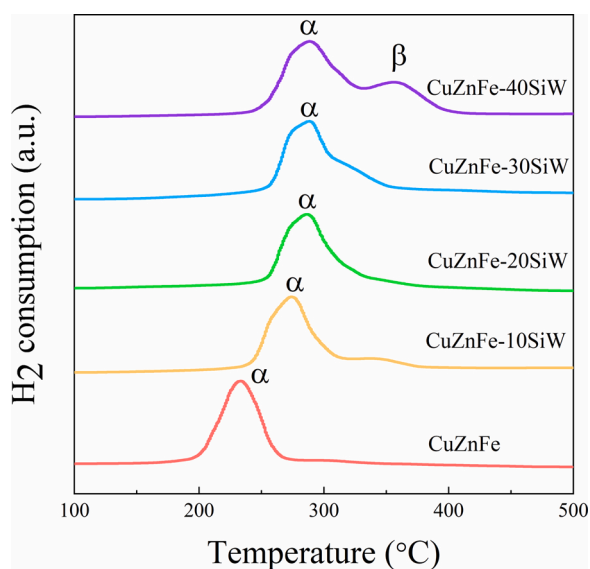


Fig. 7. H₂-TPR profiles of CuZnFe and CuZnFe-xSiW catalysts.

Table 2

Catalytic performance of various catalysts for hydrogenolysis of glycerol^a in water.

Catalyst	C _{glycerol} , %	S _{1,3-PDO} , %	Y _{1,3-PDO} , %	S _{1,2-PDO} , %	Y _{1,2-PDO} , %
CuZnFe	84.8	7.5	6.4	56.0	47.5
CuZnFe-10SiW	80.8	11.4	9.2	52.2	42.2
CuZnFe-20SiW	75.4	16.7	12.6	45.5	34.3
CuZnFe-30SiW	68.9	22.4	15.4	35.6	24.5
CuZnFe-40SiW	50.6	18.8	9.5	24.9	12.6

^a Reaction conditions: 40 wt.% glycerol solution in water (100 g), reaction temperature 220 °C, H₂ pressure (3.5 MPa), reaction time (11 h); C_{glycerol}: conversion of glycerol; S_{1,3-PDO}: selectivity to 1,3-PDO; Y_{1,3-PDO}: yield of 1,3-PDO; S_{1,2-PDO}: selectivity to 1,2-PDO; Y_{1,2-PDO}: yield of 1,2-PDO.

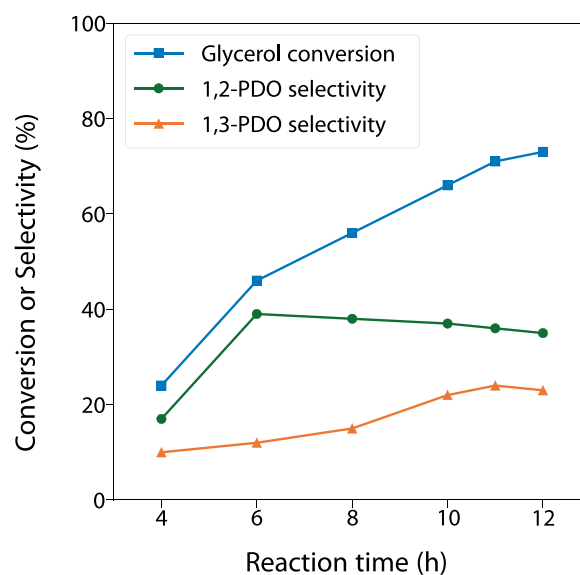


Fig. 9. Effect of reaction time on catalytic hydrogenolysis of glycerol, reaction conditions: 40 wt.% glycerol solution (100 g), reaction temperature 220 °C, reaction pressure 3.5 MPa.

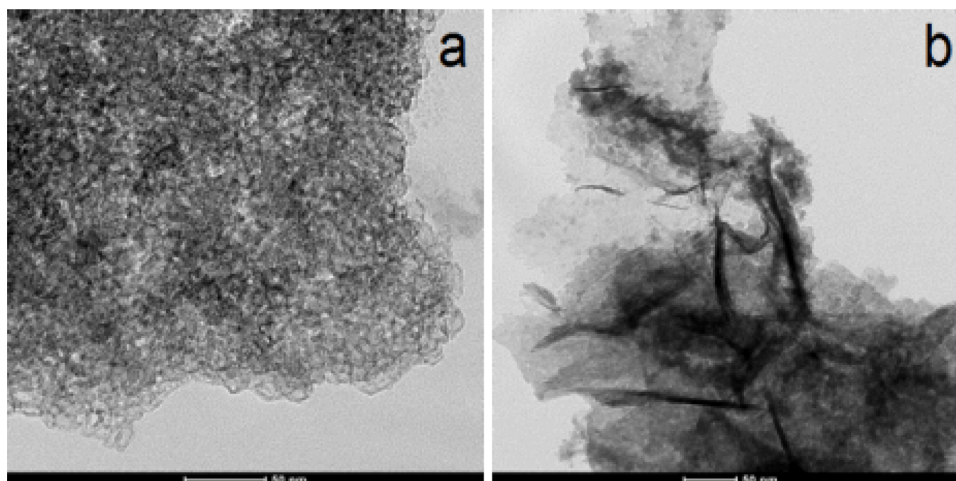


Fig. 8. TEM scans for (a) freshly reduced CuZnFe catalyst, and (b) freshly reduced CuZnFe-30SiW catalyst.

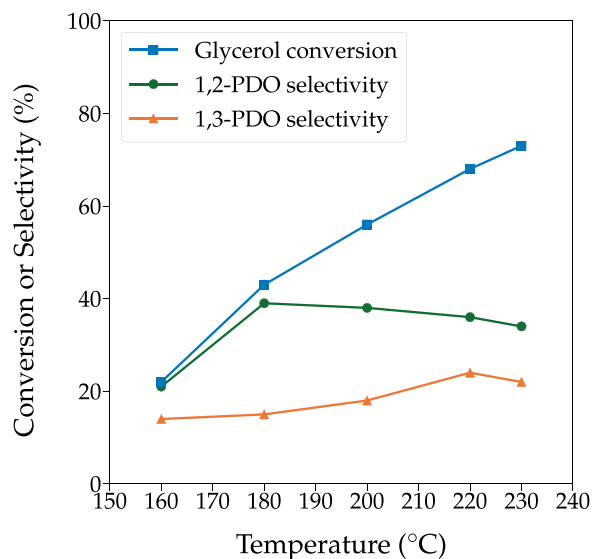


Fig. 10. Effect of reaction temperature on catalytic hydrogenolysis of glycerol, reaction conditions: 40 wt.% glycerol solution (100 g), reaction pressure 3.5 MPa, reaction time 11 h.

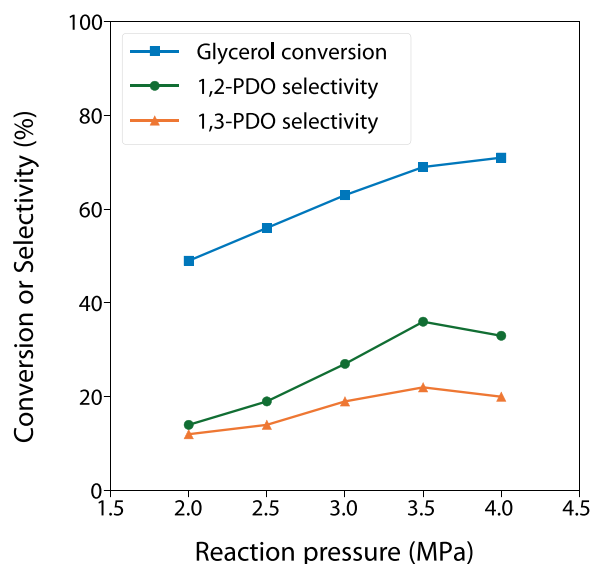


Fig. 11. Effect of hydrogen pressure on catalytic hydrogenolysis of glycerol, reaction conditions: 40 wt.% glycerol solution (100 g), reaction temperature 220 °C, reaction time 11 h.

selectivity values decreased slightly when the hydrogen pressure was elevated to 4 MPa. It indicates that 3.5 MPa was the optimal initial hydrogen pressure.

The prior BET results showed the surface area increased from 37.9 to 42.1 m²/g after the exchange of SiW with NO₃⁻. However, the pore volume and size pore changes followed an opposite trend. It implies that the diffusion of reactants has an impact of glycerol conversion. We concluded that the catalytic performance of CuZnFe-xSiW was influenced by both surface acidity and physicochemical properties. The CuZnFe-30SiW catalyst, having a good balance between surface acidity and physicochemical properties, exhibited excellent performance for 1,3-PDO production.

4. Concluding remarks

Silicotungstic acid (SiW) catalysts intercalated with CuZnFe

hydrotalcite-like compounds (HTLC) were prepared by ion-exchange method, and the successful intercalation was confirmed by XRD and FT-IR characterization. As compared with unintercalated CuZnFe, these CuZnFe-SiW catalysts derived from CuZnFeH-SiW calcination showed higher selectivity towards 1,3-PDO (1,3-propanediols), which was likely due to more Brønsted acid sites as introduced by SiW. It was found that CuZnFe-(30 wt.%) SiW exhibited the highest selectivity (22.4%) towards 1,3-PDO at 68.9% glycerol conversion under the optimal operating reaction conditions 3.5 MPa initial hydrogen pressure, 220 °C reaction temperature, and 11 h reaction time. The present work provides a promising and economical start toward technologies suitable for potential industrial scale of converting surplus glycerol to valuable propanediol chemicals.

Conflict of interest

None declared.

Declaration of Competing Interest

The authors report no declarations of interest.

Acknowledgments

We thank the National Key R&D Program of China (2019YFB1504003). We also gratefully acknowledge financial supports from the Davidson School of Chemical Engineering at Purdue University, via Varma Reaction Engineering Research Fund, and the R. Games Slayter Professorship from Dr. Arvind Varma, who initialized the collaboration between Purdue University and Southeast University.

References

- [1] A. Atabani, A. Silitonga, I.A. Badruddin, T. Mahlia, H. Masjuki, S. Mekhilef, A comprehensive review on biodiesel as an alternative energy resource and its characteristics, *Renew. Sustain. Energy Rev.* 16 (4) (2012) 2070–2093.
- [2] C.A. Quispe, C.J.J.A.C. Coronado Jr., Glycerol: production, consumption, prices, characterization and new trends in combustion, *Renew. Sustain. Energy Rev.* 27 (2013) 475–493.
- [3] Y. Xiao, G. Xiao, A. Varma, A universal procedure for crude glycerol purification from different feedstocks in biodiesel production experimental and simulation study, *Ind. Eng. Chem. Res.* 52 (39) (2013) 14291–14296.
- [4] G. Dodekatos, S. Schunemann, H. Tuysuz, Recent advances in thermo- photo-, and electrocatalytic glycerol oxidation, *ACS Catal.* (2018) 6301–6333.
- [5] N. Mimura, N. Muramatsu, N. Hiyoshi, O. Sato, Y. Masuda, A. Yamaguchi, Continuous catalytic oxidation of glycerol to carboxylic acids using nanosized gold/alumina catalysts and a liquid-phase flow reactor, *ACS Omega* 3 (10) (2018) 13862–13868.
- [6] Y. Xiao, A. Varma, Conversion of glycerol to hydrocarbon fuels via bifunctional catalysts, *ACS Energy Lett.* 1 (5) (2016) 963–968.
- [7] Y. Xiao, J. Greeley, A. Varma, Z.J. Zhao, G. Xiao, An experimental and theoretical study of glycerol oxidation to 1,3-dihydroxyacetone over bimetallic Pt-Bi catalysts, *AIChE J.* 63 (2) (2017) 705–715.
- [8] Y.C. Kim, D.J. Moon, Sustainable process for the synthesis of value-added products using glycerol as a useful raw material, *Catal. Surv. Asia* 23 (1) (2019) 10–22.
- [9] Y. Wang, Y. Xiao, G. Xiao, Sustainable Value-added C3 Chemicals from Glycerol Transformations: A Mini Review for Heterogeneous Catalytic Processes Chinese Journal of Chemical Engineering chemicals from glycerol transformations: a mini review for heterogeneous catalytic processes, *Chin. J. Chem. Eng.* 27 (2019) 1536–1542.
- [10] A. Torres, H. Shi, B. Subramaniam, R.V. Chaudhari, Aqueous-phase glycerol catalysis and kinetics with in situ hydrogen formation, *ACS Sustain. Chem. Eng.* 7 (13) (2019) 11323–11333.
- [11] Y. Ma, J. Gan, M. Pan, Y. Zhang, W. Fu, X. Duan, W. Chen, D. Chen, G. Qian, X. Zhou, Learning developers is the lack of pixel level a reaction mechanism and kinetics for Pt/CNTs catalyzed base-free oxidation of glycerol, *Chem. Eng. Sci.* 203 (2019) 228–236.
- [12] E. Vasiliadou, T. Eggenhuisen, P. Munnik, P. de Jongh, K. de Jong, A. Lemonidou, Synthesis and Performance of Highly Dispersed Cu/SiO₂ Catalysts for the Hydrogenolysis of Glycerol Applied Catalysis B, *Environmental* 145 (2014) 108–119.
- [13] D.D. Falcone, J.H. Hack, A.Y. Klyushin, A. Knop-Gericke, R. Schlogl, R.J. Davis, Evidence for the bifunctional nature of Pt-Re catalysts for selective glycerol hydrogenolysis, *ACS Catal.* 5 (10) (2015) 5679–5695.
- [14] S. Garcia-Fernandez, I. Gandarias, J. Requies, F. Soulimani, P.L. Arias, B. M. Weckhuysen, The role of tungsten oxide in the selective hydrogenolysis of

- glycerol to 1,3-propanediol over Pt/WO_x/Al₂O₃, *Appl. Catal. B: Environ.* 204 (2017) 260–272.
- [15] J. ten Dam, K. Djanashvili, F. Kapteijn, U. Hanefeld, Pt/Al₂O₃ catalyzed 1,3-propanediol formation from glycerol using tungsten additives, *ChemCatChem* 5 (2) (2013) 497–505.
- [16] A. Behr, J. Eilting, K. Irawadi, J. Leschinski, F. Lindner, Improved utilisation of renewable resources: new important derivatives of glycerol, *Green Chem.* 10 (2008) 13–30.
- [17] S. Zhu, X. Gao, Y. Zhu, J. Cui, H. Zheng, Y. Li, SiO₂ Promoted Pt/WO_x/ZrO₂ Catalysts for the Selective Hydrogenolysis of Glycerol to 1,3-propanediol Applied Catalysis B: Environmental. 158-L catalysts for the selective hydrogenolysis of glycerol to 1,3-propanediol, *Appl. Catal. B: Environ.* 159 (2014) 391–399.
- [18] C. Deng, X. Duan, J. Zhou, X. Zhou, W. Yuan, S.L. Scott, Ir-Re alloy as a highly active catalyst for the hydrogenolysis of glycerol to 1,3-propanediol, *Catal. Sci. Technol.* 5 (2015) 1540–1547.
- [19] U.I. Nda-Umar, I. Ramli, Y.H. Taufiq-Yap, E.N. Muhamad, An overview of recent research in the conversion of glycerol into biofuels, fuel additives and other bio-based chemicals, *Catalysts* 9 (1) (2019) 15.
- [20] A. Alhanash, E.F. Kozhevnikova, I.V. Kozhevnikov, Hydrogenolysis of glycerol to propanediol over Ru: polyoxometalate bifunctional catalyst, *Catal. Lett.* 120 (3) (2008) 307–311.
- [21] Y. Nakagawa, Y. Shinmi, S. Koso, K. Tomishige, Direct hydrogenolysis of glycerol into 1,3-propanediol over rhenium-modified iridium catalyst, *J. Catal.* 272 (2) (2010) 191–194.
- [22] S. Feng, B. Zhao, Y. Liang, L. Liu, J. Dong, Improving selectivity to 1,3-propanediol for glycerol hydrogenolysis using W- and Al-incorporated SBA-15 as support for Pt nanoparticles, *Ind. Eng. Chem. Res.* 58 (8) (2019) 2661–2671.
- [23] T. Kurosaka, H. Maruyama, I. Naribayashi, Y. Sasaki, Production of 1,3-Propanediol by Hydrogenolysis of Glycerol Catalyzed by Pt/WO₃/ZrO₃, *Catalysis Communications.* 9 (6) (2008) 1360–1363.
- [24] S. Garcia-Fernandez, I. Gandarias, J. Requies, M. Guemez, S. Bennici, A. Auroux, P. Arias, New approaches to the Pt/WO_x/Al₂O₃ catalytic system behavior for the selective glycerol hydrogenolysis to 1,3-propanediol, *J. Catal.* 323 (Supplement C) (2015) 65–75.
- [25] L. Niu, R. Wei, C. Li, L. Gao, M. Zhou, F. Jiang, G. Xiao, Cu/ZnO-USY: an efficient bifunctional catalyst for the hydrogenolysis of glycerol, *React. Kinetics Mech. Catal.* 115 (1) (2015) 377–388.
- [26] L. Niu, R. Wei, H. Yang, X. Li, F. Jiang, G. Xiao, Hydrogenolysis of glycerol to propanediols over Cu-MgO/USY catalyst, *Chin. J. Catal.* 34 (12) (2013) 2230–2235.
- [27] G. Geng, R. Wei, T. Liang, M. Zhou, G. Xiao, Hydrogenolysis of glycerol to propanediols on Cu-Ca-Al hydrotalcites derived catalysts, *React. Kinetics Mech. Catal.* 117 (1) (2016) 239–251.
- [28] X. Cheng, X. Huang, X. Wang, B. Zhao, A. Chen, D. Sun, Phosphate adsorption from sewage sludge filtrate using zinc-aluminum layered double hydroxides, *J. Hazard. Mater.* 169 (1) (2009) 958–964.
- [29] B.E.L. Munoz, R.R. Robles, J.L.I. Garcia, M.T.O. Gutierrez, Adsorption of basic chromium sulfate used in the tannery industries by calcined hydrotalcite, *J. Mexican Chem. Soc.* 55 (3) (2011) 137–141.
- [30] M.Q. Zhao, Q. Zhang, J.Q. Huang, F. Wei, Hierarchical nanocomposites derived from nanocarbons and layered double hydroxides - properties, synthesis and applications, *Adv. Funct. Mater.* 22 (4) (2012) 675–694.
- [31] L. Ren, J. He, S. Zhang, D. Evans, X. Duan, Immobilization of penicillin G acylase in layered double hydroxides pillared by glutamate ions, *J. Mol. Catal. B: Enzym.* 18 (1) (2002) 3–11.
- [32] F. Cavani, F. Trifiro, A. Vaccari, Hydrotalcite-type anionic clays: preparation, properties and applications, *Catal. Today* 11 (2) (1991) 173–301.
- [33] K. Parida, S. Parija, J. Das, P. Mukherjee, Preparation, Characterisation of molybdophosphoric and tungstophosphoric acid intercalated zinc aluminium hydrotalcite-like compounds and their catalytic evaluation towards the oxidative bromination of phenol, *Catal. Commun.* 7 (11) (2006) 913–919.
- [34] J. Palomeque, F. Figueras, G. Gelbard, Epoxidation with hydrotalcite-intercalated organotungstic complexes, *Appl. Catal. A: Gen.* 300 (2) (2006) 100–108.
- [35] D.P. Debecker, E.M. Gaigneaux, G. Busca, Exploring, tuning, and exploiting the basicity of hydrotalcites for applications in heterogeneous catalysis, *Chem. Eur. J.* 15 (16) (2009) 3920–3935.
- [36] G.R. Williams, D. O'Hare, Towards understanding, control and application of layered double hydroxide chemistry, *J. Mater. Chem.* 16 (2006) 3065–3074.
- [37] Z. Li, J. You, J. Wang, P. Yang, X. Jing, M. Zhang, Synthesis and characterization of tungstophosphoric acid intercalated Ni/Al HTlc with magnetite, *J. Mater. Process. Technol.* 209 (5) (2009) 2613–2619.
- [38] E. Guerreiro, O. Gorrioz, J. Rivarola, L. Arrua, Characterization of Cu/SiO₂ Catalysts Prepared by Ion Exchange for Methanol Dehydrogenation Applied Catalysis A: General catalysts prepared by ion exchange for methanol dehydrogenation, . 165 (1) (1997) 259–271.
- [39] K.T. Li, C.H. Wang, H.C. Wang, Hydrogenolysis of glycerol to 1,2-propanediol on copper core-porous silica shell-nanoparticles, *J. Taiwan Inst. Chem. Engrs.* 52 (2015) 79–84.
- [40] M. Shimokawabe, N. Takezawa, H. Kobayashi, Temperature programmed reduction of copper-silica catalysts prepared by ion exchange method, *Bull. Chem. Soc. Jpn.* 56 (5) (1983) 1337–1340.
- [41] S.S. Priya, V.P. Kumar, M.L. Kantam, S.K. Bhargava, A. Srikanth, K.V.R. Chary, High efficiency conversion of glycerol to 1,3-propanediol using a novel platinum-tungsten catalyst supported on SBA-15, *Ind. Eng. Chem. Res.* 54 (37) (2015) 9104–9115.
- [42] I. Gandarias, P. Arias, J. Requies, M. Guemez, J. Fierro, Hydrogenolysis of glycerol to propanediols over a Pt/ASA catalyst: the role of acid and metal sites on product selectivity and the reaction mechanism, *Appl. Catal. B: Environ.* 97 (1) (2010) 248–256.
- [43] L. Liu, T. Asano, Y. Nakagawa, M. Tamura, K. Okumura, K. Tomishige, Selective hydrogenolysis of glycerol to 1,3-propanediol over rhenium-oxide-modified iridium nanoparticles coating rutile titania support, *ACS Catal.* 9 (12) (2019) 10913–10930.